FATIGUE BEHAVIOR OF SPENT NUCLEAR FUEL RODS IN SIMULATED TRANSPORTATION ENVIRONMENT

Hong Wang[1]

Oak Ridge National Laboratory

1 Bethel Valley Road, PO Box 2008, MS-6069,

Oak Ridge, TN 37831, USA

Email: wangh@ornl.gov

Hao Jiang

Oak Ridge National Laboratory

1 Bethel Valley Road, PO Box 2008, MS-6069,

Oak Ridge, TN 37831, USA

Email: jiangh@ornl.gov

Jy-An John Wang

Oak Ridge National Laboratory

1 Bethel Valley Road, PO Box 2008, MS-6069,

Oak Ridge, TN 37831, USA

Email: wangja@ornl.gov

Abstract

Nuclear fuel rod is composed of cladding tube and a specified number of fuel pellets contained. In the United States, spent nuclear fuel (SNF) is expected to be transported to at least one storage facility before permanent disposal. The fatigue behavior of spent nuclear fuel (SNF) rods under reversed cyclic bending must be understood in order to evaluate their vibration integrity in a transportation environment. This is especially important for high-burnup SNFs (>45 GWd/MTU). This report presents the experimental results related to Zircaloy (Zry)-4 - based surrogate rods and high-burnup SNFs, based on recent work performed at Oak Ridge National Laboratory (ORNL). The surrogate rod was made of Zry-4 cladding and alumina pellets, and high-burnup fuel rods were discharged from H.B. Robinson pressurized water reactor. The reversed cyclic bending testing was conducted at 5 Hz under loading control. The effect of pre-hydriding and burnup or irradiation on the flexural rigidity and fatigue life of cladding-pellet system were discussed. The fatigue data obtained are extremely useful to the future certification of SNF storage and transportation cask.

1. INTRODUCTION

Shock and vibration are among the normal conditions of transport that need to be studied when spent nuclear fuel (SNF) transportation is being licensed. The licensee is required to ensure that there will be no loss or dispersal of SNF, no significant increase in external surface radiation levels, and no substantial reduction in the effectiveness of the spent fuel package [1]. Transient shock and steady vibration can impose substantial structural loading or bending to SNF rods [2], resulting in fatigue of the rods. The fatigue is exacerbated in the case of high-burnup (HBU) SNF (> 45 GWd/ MTU). The increase in the burnup of the fuel results in increases in the thickness of the cladding corrosion layer, cladding hydrogen content, cladding creep strains; release of fission gas; and formation of a HBU structure. As a result, the HBU SNF rods are susceptible to earlier failure, and their mechanical behavior needs to be carefully understood and controlled in order to satisfy regulatory requirements for shipping SNF.

The prevention of SNF release relies on the capability of cladding to contain the fuel. Fuel cladding has been studied in axial tensile tests, ring-tension tests, ring-compression tests, and biaxial tube burst tests to understand the effect of stress state and to meet the requirements of different applications. The relevant data on Zircaloy including cold-worked stress-relief annealed (CWSR or SRA) Zircaloy-4 (Zry-4) and recrystallized (RXA) Zircaloy-2 (Zry-2) were reviewed by Greelhood et al. (2008) [3], and empirical equations have been developed to describe mechanical quantities (model parameters, including elastic modulus, strength coefficient, strain-hardening exponent, strain rate exponent, and uniform elongation) as a function of variables such as fast neutron fluence, temperature, and cold work. To understand the fatigue properties of cladding materials used in the reactor core, the cyclic fatigue of Zircaloy was studied under various loading conditions, including tension and bending [4-6]. In a later study [7], it was shown that irradiation reduces the fatigue life of the materials in the lowcycle regime.

Apparently, in all of the experimental efforts, fuel cladding was studied as a stand-alone material with no fuel pellets included. This is critical because the pellet-cladding mechanical interaction (PCMI) plays a paramount role in the response of a fuel rod as a structure, as demonstrated in the related analysis on reactivity-initiated accidents (RIAs) [8,9]. Even in the case of monotonic loading, the amount of data on bending behavior of fuel rods is quite limited. A composite rod made of cladding and fuel pellets is in a highly sensitive stress state that is complicated by the combination of PCMI, the stress gradient over the cross section, and the anisotropy of the mechanical properties of the cladding (including CWSR Zry-4). The bending response of fuel cladding in such a complicated stress state remains unknown [10,11].

This report presents the results of an experimental study of the mechanical responses of fuel rods under reversed cyclic bend loadings. The rods were either fabricated from as-received and pre-hydrided Zry-4 cladding filled with alumina pellets or prepared directly from as-received H.B. Robinson (HBR) HBU SNF. The advantage of using surrogate rods is that testing parameters and testing materials are more controllable than they would be if real rods were used. The techniques described in this article were developed through recent efforts at Oak Ridge National Laboratory (ORNL) [12-14].

2. EXPERIMENTAL TECHNIQUES

2.1 Test Setup and Materials

The bending test system is mainly composed of a U-frame testing setup for imposing bending loads on the surrogate fuel rod test specimens [12]. The U-frame is equipped with two 101.60 mm loading arms; the maximum available moment of the system for bending depends on capabilities of the testing machine (e.g., ±304.80 Nm in a Bose Dual LM2 TB). The Uframe setup can accommodate 152.40 mm long rod specimens with diameters ranging from 9.50 to 11.70 mm. The rod is coupled to the U-frame using two rigid sleeves or grips that have an inside diameter (ID) of 15.00 mm, an outside diameter (OD) of 25.00 mm, and a length of 50.80 mm. The sleeves are mounted to the specimen end sections using cast epoxy. The deformation of the rods was measured by three linear variable displacement transformers (LVDTs). Use of the three LVDTs eliminated the effect of compliant layers on the deformation measurement. The effect would be significant if a single LVDT were used.

Three types of rod specimens were used in this study as shown in Table 1 and Fig. 1. ZRAP and HZRAP were surrogate rods made of as-received Zry-4 and pre-hydrided Zry-4 claddings, respectively, both with alumina pellets contained. HBR was the HBU SNF rods discharged from H.B. Robinson (HBR) pressurized water reactor (PWR) [15,16]. The average burnup of the HBR rods was from 63 to 67 GWd/MTU. The HBR fuel pellets were designed having a dish-shaped end face with a flat edge.

2.2 Test Procedure and Data Processing

The quasi-static bending tests were conducted in displacement control at a rate of 0.2 mm/s to peak value 10.00 mm at first, and then back to zero. The results of static tests were then used in planning of cyclic tests. The reversed cyclic bending tests were conducted in load control using a 5 Hz sine wave. The nominal amplitudes ranged from 10.16 to 30.48 Nm for surrogate rods and 5.08 to 35.56 Nm for HBR rods. The responses were monitored including loads, displacements of Uframe, and the deflections of rods at the three points of gauge section. The cycling was paused periodically for measurements involving three cycles of 0.05 Hz sine waves at specified amplitudes to ensure the responses of rods be captured properly. The

cyclic tests were terminated whichever of the following events occurs first: (1) the displacement of U-frame exceeds predetermined limits, or (2) the number of cycles reaches a critical value such as 1 or 2 million. Finally, the tested specimens were examined after the fatigue tests using an optical microscope (Nikon Nomarski Measure Scope MM-11, Tokyo, Japan) with focus on fracture surfaces. All tests and measurements for ZRAP/ HZRAP rods were conducted outside of hot cell at room temperature. Those for HBR rods were conducted in hot cell or irradiated fuel examination laboratory (IFEL), ORNL at room temperature.

Measurement data and on-line monitoring data were converted into moment and curvature according to the load, the loading arm length, and the deflections from three LVDTs [12,18]. The reversed cyclic bending usually results in a moment-curvature (M-κ) loop. The M-κ loop is characterized by flexural rigidity R and hysteresis UM defined by,

(1)

$$R = \frac{\Delta M}{\Delta \kappa},$$

(2)

$$U_{M} = \oint M d\kappa.$$

where ΔM and Δκ are moment and curvature ranges, respectively.

3. EXPERIMENTAL RESULTS

3.1 Fatigue Life

The results on fatigue life are summarized in Fig. 2 where moment amplitudes are presented as a function of cycles to failure (M-N). Note that the moment amplitudes (ΔM/2) are based on the measurements, which are generally a little lower than the nominal ones after de-noised.

Failure occurred only when the amplitudes were greater than 10.16 Nm in the case of surrogate rods. Within the range of loads tested, the fatigue life of ZRAP surrogate rods was found out from 2.4×10^3 to 2.2×10^6 cycles, decreasing with increasing moment as expected. The difference in fatigue life was also seen between the rods at the same amplitude, for instance, 15.24 Nm. Such difference is associated with the initial condition of the rods. Within the same range tested, the fatigue life of HZRAP rods appeared lower, particularly at high level of amplitudes. Thus, the fatigue of the rods was influenced by pre-hydriding applied to cladding.

On the other hand, the M-N plot of the HBR rods was found out to rotate clockwise. The SNF rods had a relatively longer life at the high amplitudes or in the low cycle regime (less than 105 cycles), and then became shorter at the low amplitudes. Under the amplitudes less than 8.89 Nm, the rods survived more than 6.4×10^6 cycles.

3.2 Flexural Rigidity and Hysteresis

Representative fatigue curves are given in Fig. 3 for ZRAP rods. The value of fatigued rigidity is usually related to the prefatigue level. But there was a wide range of prefatgue rigidity, which was caused by the variable initial structural condition of rods and the level of moment. The effect of initial condition on the rigidity of rod was also observed in small amplitude measurements. Several factors contribute to the varied structural condition of rods including machining of cladding tubes and pellets and bonding condition of interfaces. Meanwhile, the moment dependence of the rigidity became significant at the high level amplitudes due to nonlinear phenomenon. At 10.16 Nm, the fatigue curve of rigidity was quite flat because no appreciable degradation occurred under such level of load. For those that failed, the decrease in rigidity was observed to be significant. The fatigue rate of rigidity is associated with the moment amplitude applied; larger amplitude results in a greater falling rate in rigidity.

Overall, the prefatigue hysteresis depends on moment amplitude as shown also in Fig. 3, which is reasonable because a higher load produces a more sizable hysteresis loop in terms of both loop width and loop area. During cycling, the hysteresis itself increased in various extents and the rate of increasing became

profound at the high amplitude. At 30.48 Nm, the hysteresis was seen to surge from 6 to nearly 10 N in a short period of time because of high level loading. In general, there was an inverse correlation between the flexural rigidity and hysteresis. Similar relation was observed for SSAP rods made of modified stainless steel 304 tube and alumina pellets [19]. This is understandable because the dissipated energy of a damping system in load control can be shown to have an inverse relation to the stiffness of the system [20]. Exceptions were also seen for 20.32 Nm and 25.40 Nm. In the later stage of the cycle tests, the U_M became increasingly saturated as the loop area didn't change much even though the loop width increased.

The pre-hydriding has a significant impact on the prefatigue responses as illustrated by the reduced rigidity in Fig. 4. Except the case of 30.48 Nm, the prefatigue R values in HZRAP rods were generally quite lower than those of ZRAP rods. This appears to be contrary to the observation that the introduction of hydrogen (H) in Zry-4 cladding, for example, by an irradiation process in reactor, would have increased the elastic modulus of the cladding, and thus has a positive effect on the flexural rigidity of the rods [3]. It was also demonstrated that the ultimate tensile strength tended to decrease when the H content exceeded 600 ppm [21]; same effect is expected for elastic modulus because, at the high H content level, a denser hydride structure is formed within the metal matrix, and damage can be induced more likely in mechanical loading. So, a combination of pre-hydriding and subsequent PCMI from cyclic test would eventually deteriorate the mechanical performance of the rods as validated here. In this study, the H content of the pre-hydrided cladding was estimated ranging from 740 to 1280 ppm for the tested rods. The level of H contents may be sufficient to influence the deformation property of cladding and further the rigidity of rods in bending.

It has been also observed that, at 10.16 Nm, the R fatigue curve of the HZRAP rod exhibited a decreasing trend over the tested number of cycles, although an oscillatory response was seen as well. This is a little bit different from that of ZRAP rod. Thus, the sensible damage within surrogate rod with prehydrided cladding occurred much earlier in cyclic fatigue.

Figure 5 shows typical fatigue curves of HBR rods. The R value of SNF rods was obviously higher than those of surrogate rods, for example, at 15.24 Nm. This is partly because of a larger diameter used in

HBR rods. Additional factor is the irradiation from BHU process, with which the elastic modulus of Zry-4 cladding would be increased from 80 to 90 GPa (neutron fluence 1.2×10^{26} n/m^2, cold work 0.5) [3].

Again, a substantial variation in prefatigue R was seen in the SNF rods. Besides the level of moment amplitude as mentioned above, the variation could arise from additional aspects. First, the cladding of the SNF rods had noticeable ranges of H content from 360 to 750 ppm, and outside oxidelayer thickness from 40 to 110 μm [16]. Second, the structure of fuel pellets altered significantly after the HBU, which usually had different fracture systems in different parent rods. Finally, PCI and PPI conditions varied among the rods tested.

For HBR rods, the fatigue response of R appeared quite oscillatory or noisy during cycling. The degree of oscillation is similar to that seen in HZRAP rods and is believed to be related to the HBU structures in cladding like circumferential hydrides. However, a declining trend is still appreciable. It is interesting to see that the U_M was fairly flat in spite of the decrease in R. This is quite different from those of ZRAP and HZRAP surrogate rods shown in Figs. 3 and 4. It is suggested that, at a moment amplitude, the curvature may be increased, but the moment-curvature (M-κ) loop is still quite slender so that the loop area is maintained. The slenderness of M-κ loop of HBU SNF rods can be seen from relatively low values of U_M in Fig. 5.

3.3 Fractography

Specimens mostly failed within the nominal gauge section (50.8 mm). Crack initiation site corresponded well with the sign of peak/valley values of displacement applied on U-frame. Namely, a crack above the neutral axis of bending rod took place at the peak of displacements, and vice versa. The interfaces dominated the failure of surrogate rods. Fracture surfaces of two fracture halves are shown in Fig. 6 for one ZRAP rod as an example. The fracture occurred on a PPI as evidenced by the exposed end faces of neighboring pellets. The crack initiation site was found to be located where the PCI epoxy layer is thinner than in other areas around the circumferential direction. Alumina pellets were cracked in the two areas subjected to the largest bending stress. Detailed examinations on the cladding from both halves suggest that

the crack initiation site occurred near the inner surface of cladding as indicated by arrow; the flaw depth is less than 1/6 of wall thickness [18].

The interfaces dominated the failure of HBU SNF rods also. One of the examples is shown in Fig. 7 where failure was observed in the gauge section near motor 2 (left side) [16,22]. The failure occurred at a PPI that is identifiable readily as the end faces of two involved pellets are pretty clean. At the same time, the fracture surfaces of the cladding were serrated. Some striations were developed in the circumferential direction, but they are hardly differentiated at this magnification. Both lateral stressed sides of the rod subjected to the maximum stresses were covered with equally spaced circumferential cracks throughout the gauge section. Spalling occurred at the local area near the fracture. It is believed that the parallel equally spaced cracks were related to the preexisting condition as the rod actually had a relatively thick layer of oxidation and a high H content.

4. DISCUSSION

4.1 Fatigue Life Based on Alternative Quantities

Fatigue life data are presented for equivalent stress amplitude ($\Delta\sigma/2$) as shown in Fig. 8 to eliminate the effect of geometrical size of rods. The stresses are defined at the outer fiber of bending rods by using beam theory. So, the discussion here is more devoted to the cladding of rods. The introduced stresses tends to align the data points from different groups into a single band in the low cycle regime ($<10^5$ cycles), although the data points are still too few to make a clear observation. A knee point exists; fatigue limit can be identified around 115 MPa for Zry-4 cladding in ZRAP/HZRAP and 70 MPa in HBR rods.

The fatigue life is characterized also using amplitude of equivalent strain ($\Delta\varepsilon/2$) as shown in Fig. 9. Similar to the equivalent stresses, the equivalent strains were defined at the outer fiber of bending rod according to beam theory, and calculated directly from curvatures. Note that the cyclic tests were performed in moment control. So, the strain was output varying during cyclic test due to the fatigue as focused in this study, the evaluation of which was based on the average of monitoring data in individual test. The use of strain amplitudes did separate the data points of ZRAP/ HZRAP rods from those of HBR rods, but not from

each other. The distance of ZRAP/ HZRAP data points from those of HBR in ε-N plots is understandable in light of relatively high level of rigidity as seen in Figs. 3-5.

The HBR rods showed a lower life than ZRAP/ HZRAP rods. The effect of irradiation on the fatigue life of Zry-4 cladding observed in this study is similar to those obtained on Zry-2 cladding by Wisner et. el. [7].

Meanwhile, strain fatigue limit was found near 0.15% in ZRAP rods and 0.06% in BHR rods. The fatigue limits are lower than those obtained of Zry-2, 0.22% [4] and 0.18% [6]. Several important factors account for the observed discrepancy. First, the chemical composition difference between two alloys is apparently the primary contributing factor to the difference observed. Second, the irradiated cladding in HBR rods deforms in a much more heterogeneous manner. The dense circumferential hydrides are generally located near the subsurface and inside a significant part of cladding wall. The hydrides are relatively brittle compared to metal matrix, and have a tendency to fail earlier at an elongation. The outside oxide layer is inherently brittle too and can be readily a failure initiation site for a cladding tube in bending. Third, the cladding in HBR rods is complicated tremendously by the PCIs/ PPIs which are the sources of stress concentration. The effect of pellets on the fatigue of cladding essentially cannot be evaluated by testing cladding only. Namely, the fatigue limits reported for both unirradiated and irradiated Zry-2 don't reflect the effects of related PCMI process. Nevertheless, the results obtained in this study showed that a fatigue limit can be established for Zry-4 in HBU rods.

4.2 Equivalent Modulus

The difference in rigidities between the ZRAP and HBR rods deserves to be commented. As mentioned, such difference is attributed to several important aspects, including cross sectional size of rods and irradiation effect on cladding. Tight bonding of PCIs in the HBR rods enhanced the rigidity as well. On the other hand, the HBR pellets had a smaller length in design and were usually fractured after the HBU. The latter two aspects may cause the rigidity to decrease; however, the negative effect was insignificant. The flexural rigidities [based on Eq. (1)] were converted subsequently into equivalent elastic moduli (E) of

cladding to illustrate the effects of irradiation and fuel pellets, and the results are presented as a function of cycles to failure in Fig. 10. Again, the rigidity was evaluated as an average of monitoring data for related test (Figs. 3-5). Thus, the results presented shall more or less contain the effect of fatigue, depending on the rate of degradation.

In general, the rods tested at a low-moment amplitude had a high modulus, corresponding to a long fatigue life as expected. Interestingly, the theoretically-predicated elastic moduli of Zry-4 cladding for the as-received and the HBU (as highlighted by the arrows at 80 and 90 GPa, respectively) are, in fact, located at the middle of respective data groups for ZRAP and HBR. It is also seen that the moduli of HZRAP rods are relatively low. It may be related to the pre-hydriding process or the high H content injected as mentioned in Sect. 3.2.

4.3 Fatigue Mechanism

The fatigue-induced degradation of flexural stiffness generally has a primary stage, a secondary stage, and a tertiary stage. The primary stage of fatigue was usually not seen in this study because ramping load to a designed level of amplitude took time. The secondary stage is extended over most of the fatigue process; fatigue of material in this stage is attributed to microcrack activities in pellets and cladding, debonding of PPIs and PCIs, etc. The tertiary stage is quite short for the rods tested because the propagation of crack is unstable in load control. The rigidity fatigue response shall be predicted properly once its response is characterized.

The previous work showed that irradiated Zircaloy deforms by a dislocation channeling mechanism [7,23]; however, details of the process is not available for fatigued Zircaloy. The discussion may be referred to earlier work in irradiated copper [24] which showed that cyclic strain was accommodated within a limited number of dislocation channels, resulting in large slip steps at the surface. These slip steps serve as fatigue crack initiation sites. The Zircaloy materials used in the previous fatigue studies may be exposed to various levels of fluence in an environment. But the exposure has barely reached as high as that in HBU HBR rods. The prevailing circumferential hydrides and oxide corrosion layer in the latter were not reported in the

previous efforts. However, these heterogeneous structures are extremely important to the fatigue performance of cladding.

The triple junction formed by PCI and PPI dominates the fatigue failure. In some sense, a PPI represents a structural defect to the bending rod. The numerical study illustrated that, within the cladding, the stress concentration factor Kt can be as high as 2.60 near PPI in the gauge section of rod [25]. The maximum stress may occur on the inside surface or outside surface of cladding, depending on the bonding efficiency on the PCI. In the past, fatigue data were published on Zry-4 [7], but not enough to construct a complete S-N curve for a clear definition of fatigue limit. As mentioned above, extensive experiments were conducted on Zry-2. The fatigue limits for unirradiated and irradiated Zry-2 were identified to be 171 MPa and 177 MPa, respectively [4]. If using the fatigue data of Zry- 2 as a reference, the fatigue notch factor Kf (as ratio of smooth fatigue limit to notched fatigue limit at 5×10^6 cycles) were found out to be 1.49 and 2.53 for unirradiated (ZRAP) and irradiated (HBR) Zry-4 claddings, respectively.

The fatigue mechanism of SNF rods under transportation environment remains to be explored. To study this and other technical issues on SNF rods in hot cell has not been shown to be feasible in terms of setup accessibility, fuel availability, and operational cost. Use of surrogate rods has been seen to be effective in addressing this challenge. Particularly, it has been demonstrated that the ZRAP/ HZRAP rods can capture major failure mechanisms like the PCMI as observed in HBU SNF rods. This is significant because that suggests that testing and characterization approaches developed by using surrogate rods may be migrated onto real fuel rods.

5. CONCLUSION

The reversed cyclic bending tests were conducted on ZRAP/ HZRAP rods made of as-received and pre-hydrided Zry-4–cladding tubes and alumina pellets, and HBR HBU SNF rods. The fatigue tests covered a wide range of moment amplitudes from 10.16 to 30.48 Nm for ZRAP/ HZRAP rods and 5.08 to 35.56

Nm for HBR rods. The fatigue cycles were accumulated to as high as 2.20×10^6 for ZRAP rods and 2.24×10^7 for HBR rods. The conclusions drawn based on the test results and data analysis are as follows:

1. Fatigue failure was observed only when the moment amplitude was higher than 10.16 Nm for ZRAP/ HZRAP rods and 7.62 Nm for HBR rods. Fatigue limits exist in the Zry-4 cladding; namely, 115 MPa for ZRAP rods and 70 MPa for HBR rods.
2. The PPI and PCI dominated the failure of the rod under reversed cyclic bending. The failure of cladding generally occurred near one of the PPIs.
3. There was a degradation of flexural rigidity under reversed cyclic bending. The degradation was related to the applied moment amplitude and the pre-existing condition of the rod.
4. Both equivalent stress and strain offered an effective characterization of fatigue lives of ZRAP and HBR rods. The equivalent elastic moduli of ZRAP and SNF Zry-4 claddings were distributed around the estimated moduli of the unirradiated and irradiated claddings, respectively.

ACKNOWLEDGMENTS

The research was jointly sponsored by the Office of Nuclear Regulatory Research, U.S. Nuclear Regulatory Commission (NRC), and U.S. Department of Energy (DOE) Used Fuel Disposition Campaign programs under DOE contract DE-AC05-00OR22725 with UT-Battelle, LLC. The authors would like to thank NRC program managers Michelle Bales and Patrick Raynaud, ORNL program managers Bruce Bevard and Rob Howard, and Pacific Northwest National Laboratory program manager Harold Adkins for providing guidance and support. The authors are grateful to Charles Baldwin, Yong Yan, Randy Parten, Bryan Woody, and Jeffery Thurman of ORNL for their help.

REFERENCES

[1] NRC, 2010, "Part 71, Packaging and Transportation for Radioactive Material," General Standards for All Packages, §43(f) in Title 10, Code of Federal Regulations, US Nuclear Regulatory Commission, Washington, DC.

[2] Sanders, T. L., Seager, K. D., Rashid, Y. R., Barrett, P. R., Malinauskas, A. P., Einziger, R. E., Jordan, H., Duffey, T. A., Sutherland, S. H., Reardon, P. C., 1992, "A Method for Determining the Spent-Fuel Contribution to Transport Cask Containment Requirements," SANDSO-2406, Sandia National Laboratory, Albuquerque, NM.

[3] Geelhood, K. J., Beyer, C. E., Luscher, W. G., 2008, "PNNL Stress/Strain Correlation for Zircaloy," PNNL-17700, Pacific Northwest National Laboratory, Richland, WA.

[4] O'Donnell, W. J., Langer, B. F., 1964, "Fatigue Design Basis for Zircaloy Components," Nucl. Sci. and Eng., 20, pp. 1- 12.

[5] Pettersson, K., 1975, "Low-Cycle Fatigue Properties of Zircaloy-2 Cladding," J. Nucl. Mater., 56, pp. 91-102.

[6] Nakatsuka, M., Kubo, T., and Hayashi, 1991, Y., "Fatigue Behavior of Neutron Irradiated Zircaloy-2 Fuel Cladding Tubes," Zirconium in the Nuclear Industry: Ninth Int. Symp., ASTM STP 1132, C. M. Eucken and A. M. Garde, Eds., American Society for Testing and Materials, Philadelphia, PA, pp. 230-245.

[7] Wisner, S. B., Reynolds, M. B., and Adamson, 1994, R. B., "Fatigue Behavior of Irradiated and Unirradiated Zircaloy and Zirconium," Zirconium in the Nuclear Industry: Tenth Int. Symp., ASTM STP 1245, A.M. Garde and E. R. Bradley, Eds., American Society for Testing and Materials, Philadelphia, PA, pp. 499-520.

[8] Fuketa, T., Sasajima, H., Sugiyama, T., 2001, "Behavior of High-Burn-Up PWR Fuels with Low-Tin Zircaloy-4 Cladding under Reactivity-Initiated-Accident Conditions," Nucl. Technol., 133, pp. 50-62.

[9] Tomiyasu, K., Sugiyama, T., and Fuketa, T., 2007, "Influence of Cladding-Peripheral Hydride on Mechanical Fuel Failure under Reactivity-Initiated Accident Conditions," J. Nucl. Sci. and Tech., 44, pp. 733-742.

[10] Link, T. M., Koss, D. A., and Motta, A. T., 1998, "Failure of Zircaloy Cladding under Transverse Plane-Strain Deformation," Nucl. Eng. and Des., 186, pp. 379 – 394.

[11] Saux, M. Le, Besson, J., Carassou, S., Poussard, C., Averty, X., 2010, "Behavior and Failure of Uniformly Hydrided Zircaloy-4 Fuel Claddings between 25oC and 480oC under Various Stress States, Including RIA Loading Conditions," Eng. Fail. Anal., 17, pp. 683-700.

[12] Wang, H., Wang, J.-A. J., Tan, T., Jiang, H., Cox, T. S., Howard, R. L., Bevard, B. B., and Flanagan, M. E., 2013, "Development of U-Frame Bending System for Studying the Vibration Integrity of Spent Nuclear Fuel," J. Nucl. Mater., 440, pp. 201-213.

[13] Wang, J.-A. J., Wang, H., Cox, T., Baldwin, C., 2013, "Progress Letter Report on Bending Fatigue Test System Development for Spent Nuclear Fuel Vibration Integrity Study (Out-of-Cell Fatigue Testing Development – Task 2.4)," ORNL/TM-2013/225, Oak Ridge National Laboratory, Oak Ridge, TN.

[14] Wang, J.-A., Wang, H., Bevard, B., and Howard, R., 2014, "New Rig for Studying SNF Vibration Integrity," Nucl. Eng. Int., 59, pp. 36-37.

[15] Ruzauskas, E. J., and Fardell, K. N., 2001, "Design, Operation, and Performance Data for High Burnup PWR Fuel from H. B. Robinson Plant for Use in the NRC Experimental Program at Argonne National Laboratory," 1001558, Electric Power Research Institute, Palo Alto, CA.

[16] Wang, J.-A., Wang, H., 2015, "Mechanical Fatigue Testing of High-Burnup Fuel for Transportation Applications," NUREG/CR-7198/ORNL/TM-2014/214, Oak Ridge National Laboratory, Oak Ridge, TN.

[17] Yan, Y., 2011, "Hydrogen Charging Techniques Being Developed at ORNL and Results to Date," NRC Spent Fuel Vibration Program Review Meeting, Oak Ridge National Laboratory, Oak Ridge, TN.

[18] Wang, H., Wang, J.-A. J., 2016, "Bending Testing and Characterization of Surrogate Nuclear Fuel Rods Made of Zircaloy-4 Cladding and Aluminum Oxide Pellets," J. of Nucl. Mater., 479, pp. 470-482.

[19] Wang, H., Wang, J.-A. J., 2017, "Experimental Study on Surrogate Nuclear Fuel Rods under Reversed Cyclic Bending," Fatigue and Fracture Test Planning, Test Data Acquisitions, and Analysis, ASTM STP 1598, Z. Wei, K. Nikbin, P. McKeighan, and G. Harlow, Eds., ASTM International, West Conshohocken, PA, pp. 19–36.

[20] Thomson, W. T., 1993, Theory of Vibration with Applications, 4th Edition, Prentice Hall, Upper Saddle River, NJ, Chap 3.

[21] Kim, J. H., Lee, M. H., Choi, B. K., Jeong, Y. H., 2006, "Effects of Oxide and Hydrogen on the Circumferential Mechanical Properties of Zircaloy-4 Cladding," Nucl. Eng. and Des., 236, pp. 1867-1873.

[22] Baldwin, C., 2013, "NRC Fuel Test Photos," Oak Ridge National Laboratory, Oak Ridge, TN.

[23] Adamson, R. B., Wisner, S. B., Tucker, R. P., and Rand, R. A., 1986, "The Use of Small-Scale Specimens for Testing Irradiated Materials," ASTM STP 888, W. R. Corwin and L. E. Lucas, Eds., American Society for Testing and Materials, Philadelphia, 1986, pp. 171-185.

[24] Adamson, R. B., 1968, "Cyclic Deformation of Neutron Irradiated Copper," Philosophical Magazine, 17, p. 681- 693.

[25] Jiang, H., Wang, J.-A. J., Wang, H., 2014, "Potential Impact of Interfacial Bonding Efficiency on Used Nuclear Fuel Vibration Integrity during Normal Transportation," Proc. of the ASME 2014 Pressure Vessels & Piping Conference, Anaheim, CA. Paper No. PVP2014-29067.

Table 1 Specifications of specimens

Specimen type	Cladding	Pellets	Interface*	Comments
ZRAP	As-received Zry-4: OD 9.50 mm, ID 8.36 mm, length 152.40 mm	Alumina, dia 7.94 mm, length 15.24 mm	PCI, PPI: epoxy bonding	Surrogate rods
HZRAP	Pre-hydrized Zry-4: OD 9.50 mm, ID 8.36 mm, length 152.40 mm; hydrogen content 740 to 1280 ppm [17]	Alumina, dia 7.94 mm, length 15.24 mm	PCI, PPI: epoxy bonding	Surrogate rods
HBR	HBU Zry-4: OD 10.76 mm, ID 9.26 mm, length 152.40 mm; hydrogen content 360-800 pm [15,16]	UO_2 : dia 9.06 mm, length 6.93 mm	PCI: tight bonding; PPI: tight bonding around edge.	HBR SNF rods

* PCI stands for pellet-to-cladding interface; PPI stands for pellet-to-pellet interface.

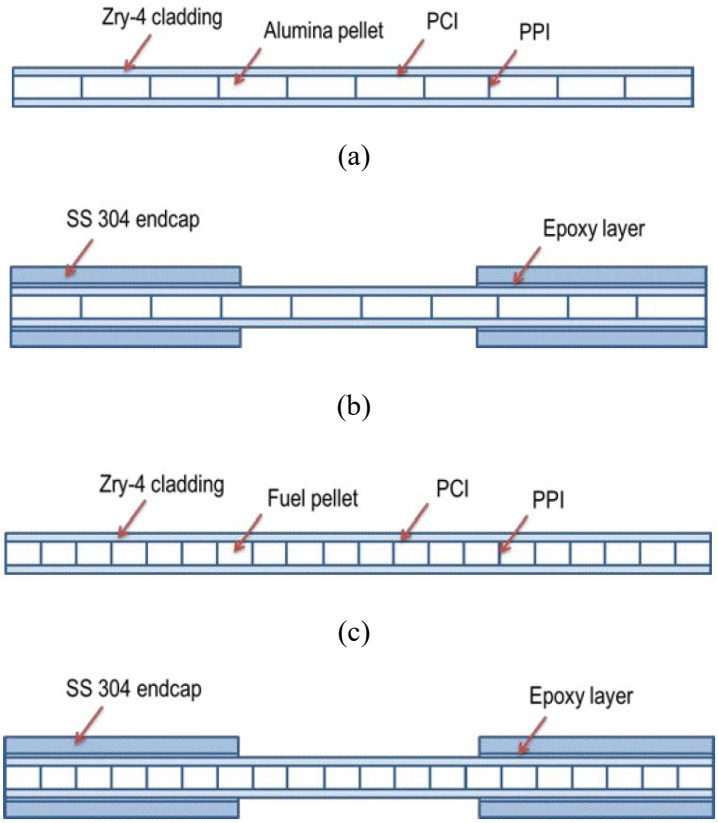

Figure 1. Schematic showing un-capped and endcapped rods for (a-b) ZRAP/ HZRAP, and (c-d) HBR; drawings are not to the scale. PCI stands for pellet-to-cladding interface; PPI stands for pellet-to-pellet interface.

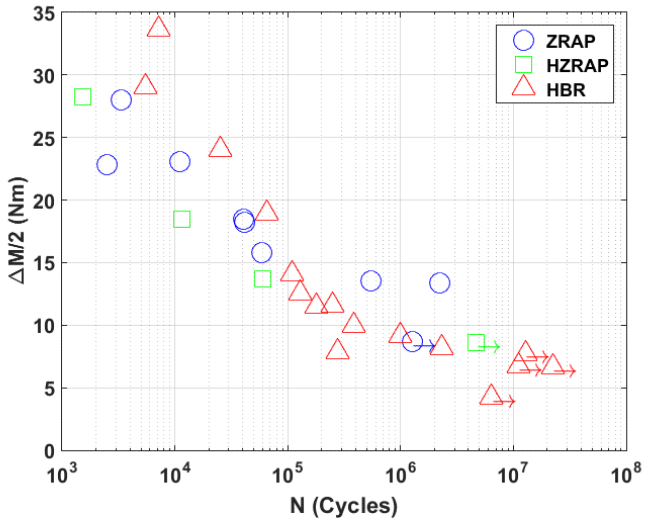

Figure 2. M-N relations based on reversed cyclic tests for all specimens. The symbols with arrow indicate that the tests were stopped without failure.

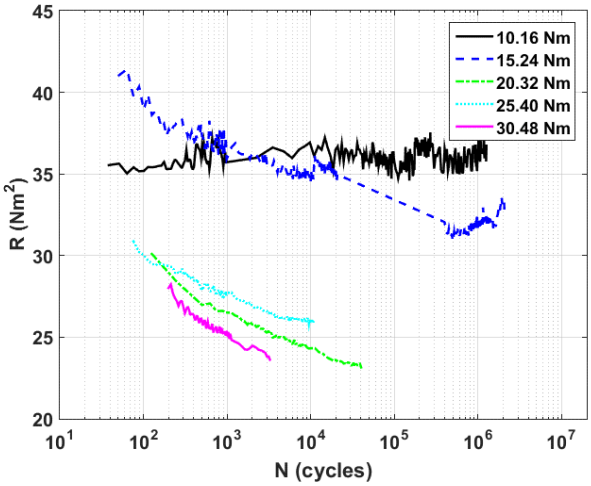

(a)

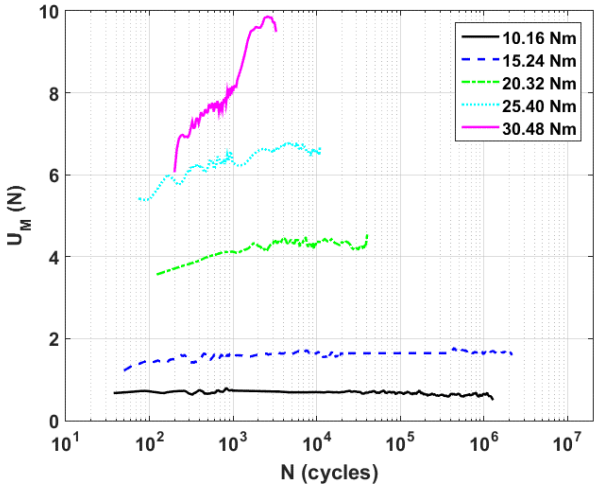

(b)

Figure 3. Variations of (a) flexural rigidity and (b) hysteresis as a function of cycle number under various moment amplitudes; ZRAP specimens. The test under 10.16 Nm was stopped.

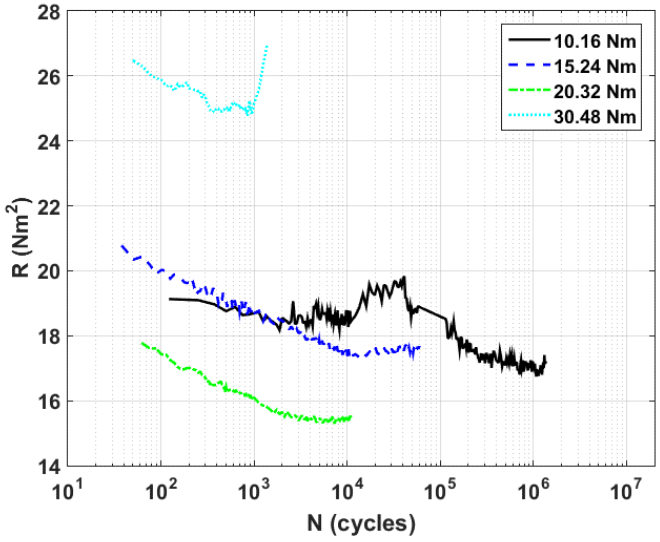

(a)

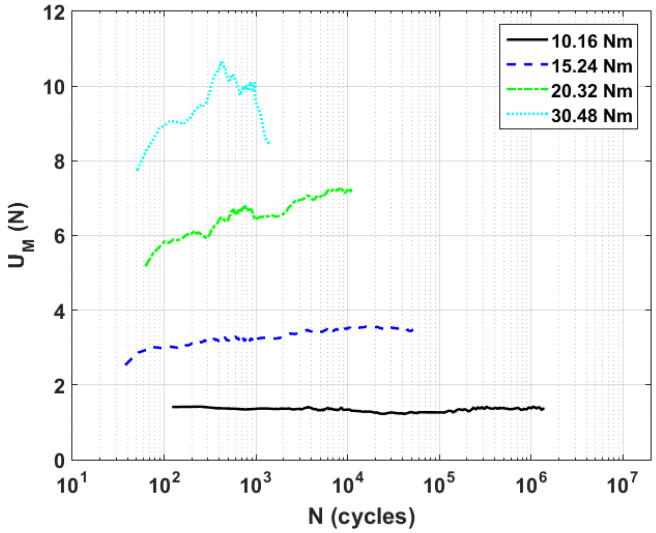

(b)

Figure 4. Variations of (a) flexural rigidity and (b) hysteresis as a function of cycle number under various moment amplitudes; HZRAP specimens. The test under 10.16 Nm was stopped.

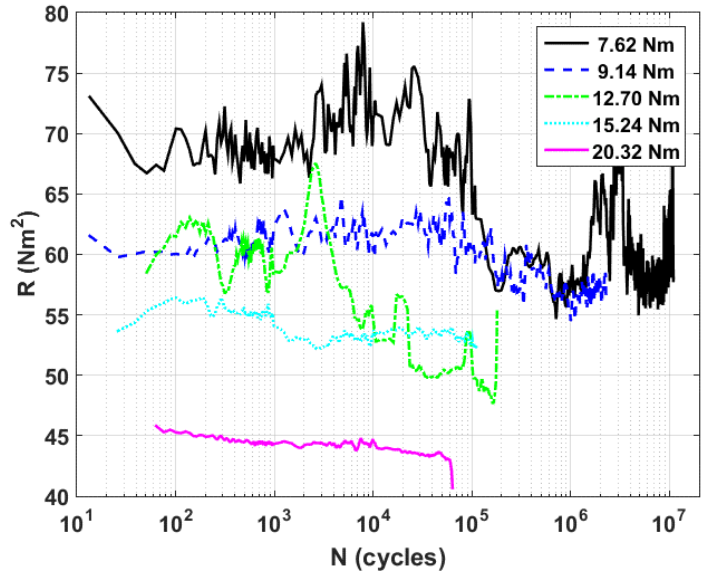

(a)

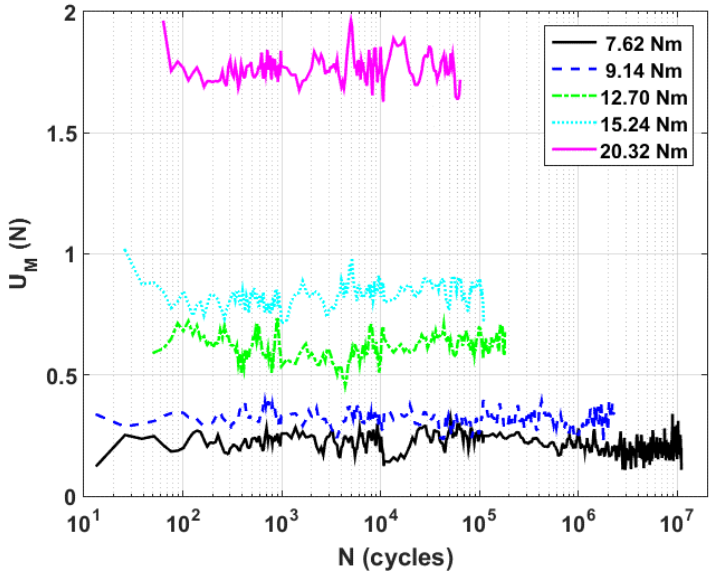

(b)

Figure 5. Variations of (a) flexural rigidity and (b) hysteresis as a function of cycle number under various moment amplitudes; HBR specimens. The test at 7.62 Nm was stopped.

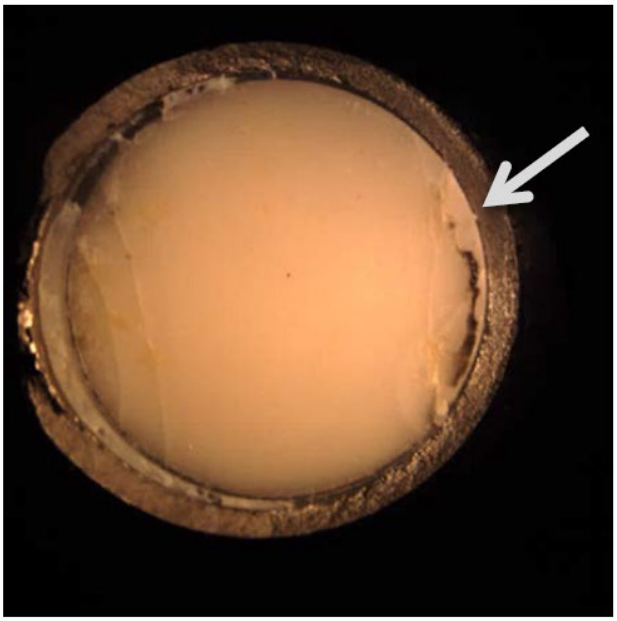

(a)

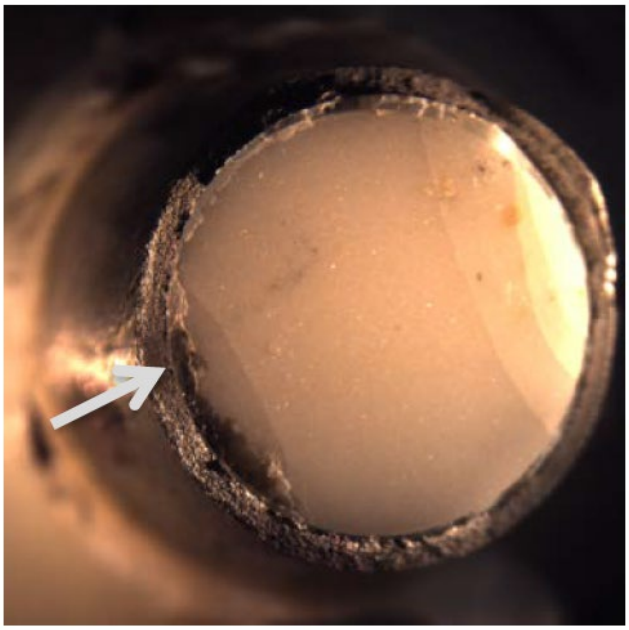

(b)

Figure 6. (a) and (b) Mating fracture surfaces of a ZRAP rod under 15.24 Nm that failed at 2.2×10^6 cycles; failure occurred on a PPI; failure origin location is indicated by an arrow.

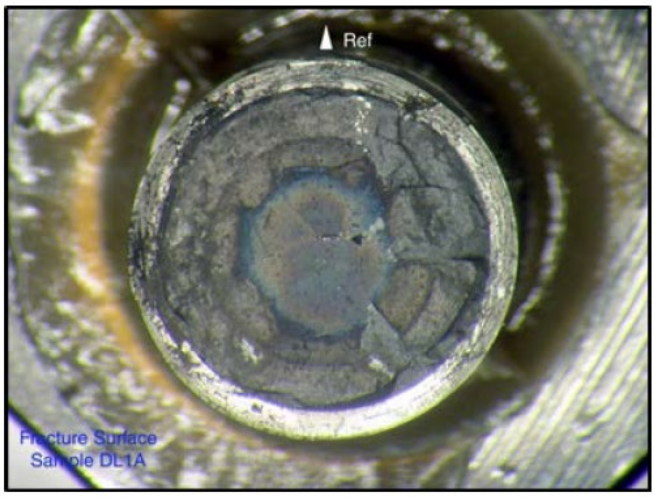

(a)

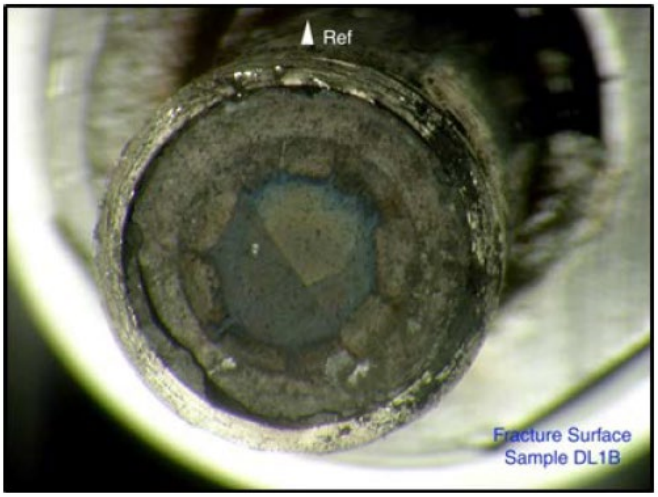

(b)

Figure 7. (a) and (b) Mating fracture surfaces of a HBU HBR rod, Nf = 1.1×10^5 cycles under ±15.24 Nm 5 Hz [16,22].

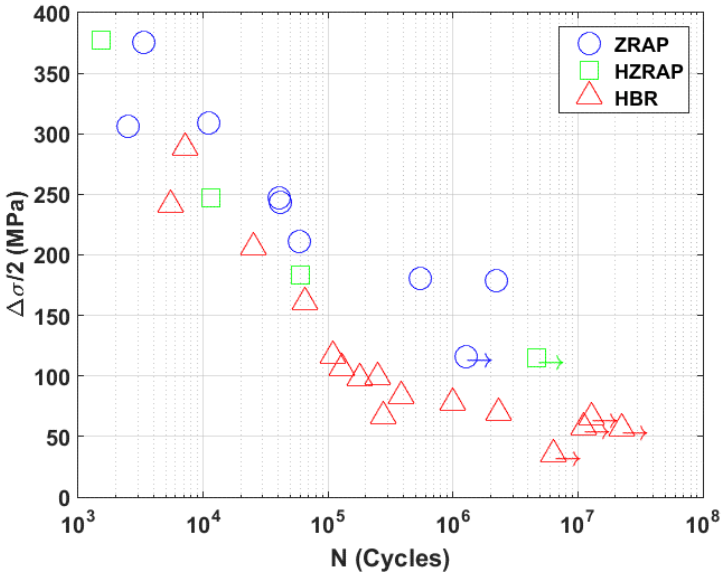

Figure 8. σ-N relations based on reversed cyclic tests for all the specimens. The symbols with arrow indicate that the tests were stopped without failure.

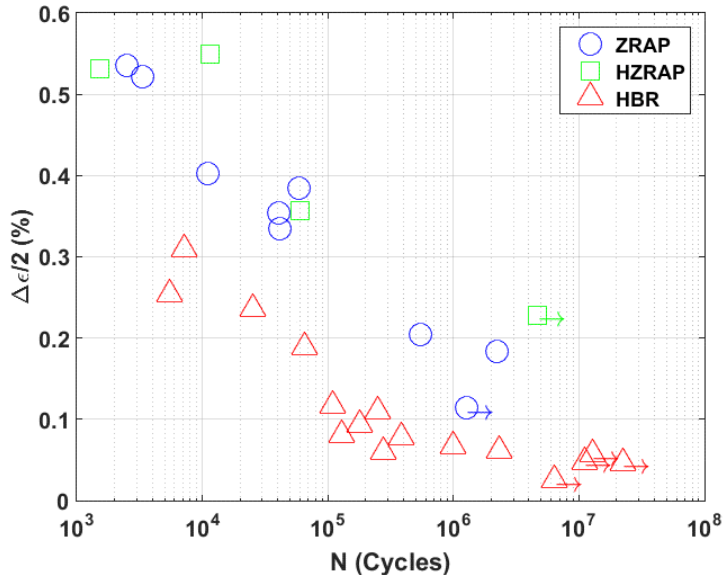

Figure 9. ε-N relations based on reversed cyclic tests for all the specimens. The symbols with arrow indicate that the tests were stopped without failure

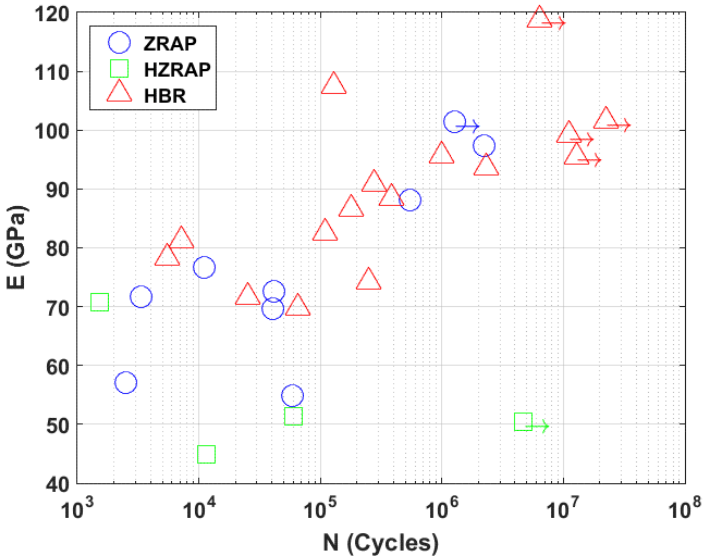

Figure 10. E-N relations based on reversed cyclic tests for all the specimens. The symbols with arrow indicate that the tests were stopped without failure.